A Dual-Band HF and UHF Antenna System for Implanted Neural Recording and Stimulation Devices

Apoorva Sharma, *Student Member, IEEE*, Eleftherios Kampianakis, *Student Member, IEEE*, and Matthew S. Reynolds, *Senior Member, IEEE*

***Abstract*—We present a dual-band high-frequency (HF) and ultrahigh-frequency (UHF) (13.56 and 902–928 MHz) antenna system for implanted neural recording and/or stimulation devices. This system consists of implant-side and external antennas. These antennas are intended for dual-band systems, where power is supplied to the implant via inductive coupling in the HF band, while data are transferred via UHF near-field coupling. The antenna system consists of an implant-side antenna of 25 mm diameter and 3 mm thickness, as well as an external antenna of 85 mm diameter and 3 mm thickness. We present both time- and frequency-domain simulation results for antenna performance and specific absorption rate in a layered tissue model, as well as experimental confirmation of antenna performance in a saline tissue proxy. With an implant depth of 11 mm and an air gap of 5 mm, the power link has a 17% measured power transfer efficiency in the HF band, inclusive of matching component losses, and the UHF communication link has 38-dB insertion loss over the 902–928-MHz band.**

***Index Terms*—Biomedical telemetry, implantable biomedical devices, implanted antennas.**

I. Introduction

IMPLANTED biomedical devices for neural recording and/or stimulation face two key challenges: remaining powered over a long duration, and communicating with an external system with sufficient bandwidth. These two requirements drive the design of the implanted antenna system. Typical implanted devices [1]–[3] have volume on the order of a few mm^3 to a few cm^3, limited by allowable tissue displacement, and a power budget on the order of μW to mW, limited by tissue heating. The communication bandwidths required increase with the number of supported electrodes; given reasonable assumptions about sampling rate and resolution, data rates into the tens to hundreds of Mbps are required for high-density probes with dozens of electrodes [4].

It is well known that the optimal choice of operating frequency for transferring power in an implanted device is a function of the size of the implanted system as well as the electromagnetic properties of the tissue in which it is embedded [5], [6]. For neural recording and stimulation in larger rodents or primates, with implants in the ≈ 1 cm^3 volume class, transferring wireless power in the high-frequency (HF) spectrum (e.g., 13.56 MHz) represents a good compromise between antenna size and efficiency. To support data rates in the tens to hundreds of Mbps, a communication link in the ultrahigh-frequency (UHF) spectrum (e.g., 915 MHz) is a common choice, due to the very limited bandwidth available in the HF spectrum. This results in the overall system block diagram of Fig. 1.

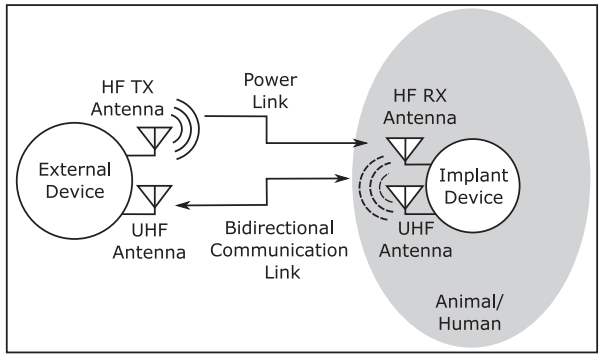

Fig. 1. Dual-band power and communication system concept.

Because both the implanted and external devices must support both bands while being as compact as possible, we have designed them as dual-band integrated planar structures. The implant antenna is a three-layer structure with an internal ground plane and buried vias. This stackup permits implanted electronics to be placed on the back side of the antenna to minimize the total volume of the implant. The implanted antenna is laminated with 1-mm-thick Teflon on the top and bottom of the stack, yielding a total size of 25 mm diameter and 3 mm thickness. The 25-mm-diameter constraint is driven by the dimension of the electrocorticography electrode array used in interventional epilepsy surgeries [7]. The structure of the external antenna allows the matching components to be integrated on the back of a simpler two-layer printed circuit. A photograph of the fabricated antennas is shown in Fig. 2, while a plan-view rendering of the active structures is shown in Fig. 3.

The antennas were simulated in the layered biomodel of Fig. 2, using time- and frequency-domain solvers (CST, Inc.), and then fabricated and tested in a saline tissue proxy. The layer model is similar to that used to design prior neural implants

Manuscript received December 14, 2015; revised June 17, 2016; accepted June 23, 2016. Date of publication June 28, 2016; date of current version March 13, 2017. This work was supported by the National Science Foundation under Award EEC-1028725. This letter does not necessarily represent the official views of the National Science Foundation.

A. Sharma and E. Kampianakis are with the Department of Electrical Engineering, University of Washington, Seattle, WA 98195 USA (e-mail: apoorvas@uw.edu; ekampian@uw.edu).

M. S. Reynolds is with the Department of Electrical Engineering and the Department of Computer Science and Engineering, University of Washington, Seattle, WA 98195 USA (e-mail: matt.reynolds@ee.washington.edu).

Color versions of one or more of the figures in this letter are available online at http://ieeexplore.ieee.org.

Digital Object Identifier 10.1109/LAWP.2016.2585650

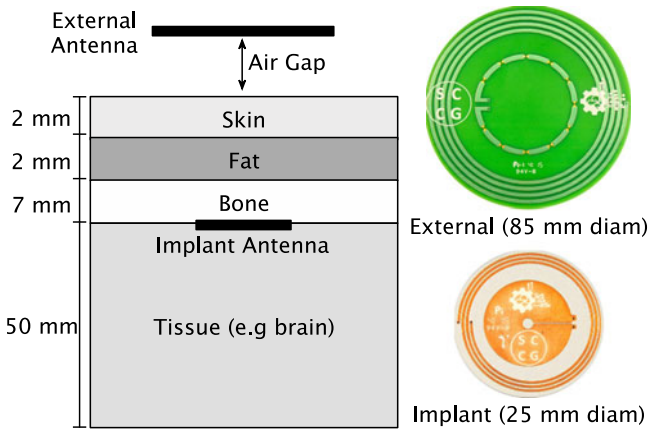

Fig. 2. Layer model and photographs of fabricated external and implant antennas.

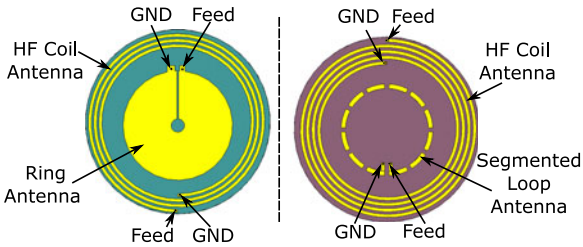

Fig. 3. Plan views of the (a) implant antenna and (b) external antenna.

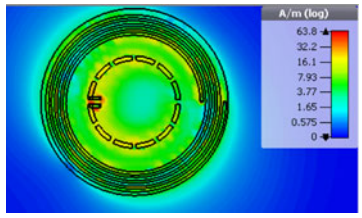

Fig. 4. HF matching network for external and implant antennas.

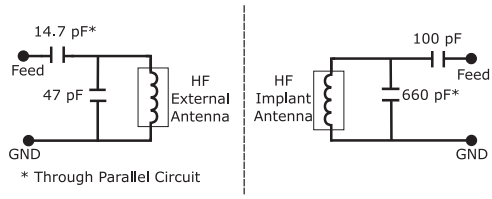

Fig. 5. H-field uniformity of external segmented loop antenna, 915 MHz.

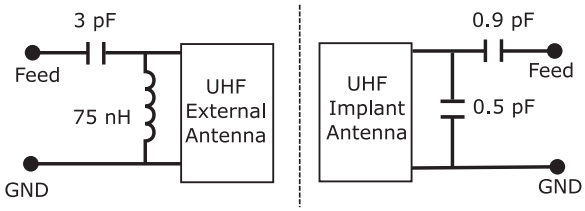

Fig. 6. Layer stackup of implant antenna.

[8], while the dielectric properties of each layer were calculated using parametric models [9].

II. Design of the External Antenna

As shown in Fig. 2, the dual-band external antenna is designed for placement external to the outermost tissue layer, with a nominal 5-mm air gap between the inner surface of the external antenna and the outer surface of the skin. As shown in Fig. 3, it has a concentric arrangement of HF (outer annulus) and UHF (inner ring) antenna elements fabricated on a two-layer printed circuit, 85 mm in diameter with 2-mm-thick FR-4 substrate and 70-μm copper thickness. The antenna is laminated between 0.4-mm-thick Teflon sheets, yielding overall dimensions of 85 mm diameter $\times$ 3 mm thickness.

The HF antenna consists of a four-turn continuous spiral loop with outer radius 41.6 mm and inner radius 29.8 mm. The trace width is 1.4 mm and the interturn spacing is 1.2 mm. These trace and space parameters were optimized using the frequency-domain solver in CST to maximize the efficiency (using the transducer gain formula described in Section V) from the external HF antenna to the implanted HF antenna, given the layered biomodel and the nominal 5-mm air gap.

A segmented loop UHF antenna structure was chosen for two reasons. First, unlike a continuous loop where the circumference is comparable to the guided wavelength, segmented loops can be engineered to yield a relatively uniform H-field within the diameter of the loop, as shown in Fig. 4. Second, because each segment of the loop is separated by capacitors, the current induced in the UHF loop by the surrounding HF coil can be more easily managed. This allows the unwanted interaction between the two concentric antenna elements to be reduced when compared to the alternative of a continuous (nonsegmented) inner UHF loop.

The segmented loop diameter is 42 mm, with trace width of 2 mm. Murata 36-pF lumped capacitors (part number GRM1555C1H360GA01D) were used between each of the 11 segments. The capacitor value was chosen by a parameter sweep in CST to yield a uniform current distribution by compensating the phase shift along the loop, which leads to a more uniform H-field distribution while simultaneously suppressing the radiated E-field component and thus reducing the specific absorption rate (SAR) in the adjacent tissue [10]. Capacitor package parasitics were significant and thus included in the model when performing the parameter sweep. The lumped element matching networks shown in Figs. 5 and 6 are employed to reduce the required board area compared to printed (e.g., microstrip) matching elements.

III. Design of the Implant Antenna

As shown in Fig. 7, the implanted device consists of three copper layers and three dielectric layers. The top copper layer is used for the HF and UHF antenna structures, while the bottom copper layer is used for matching components and to accommodate future integrated data acquisition electronics. The middle layer is a ground plane separating the antenna structures on the top layer from the electronics on the bottom layer. This stackup supports both through-vias as well as buried vias between copper layers 2 and 3. Through-vias connect the top layer to the bottom layer at the feed points, while buried vias tie ground nets on the bottom layer to the inner ground layer without

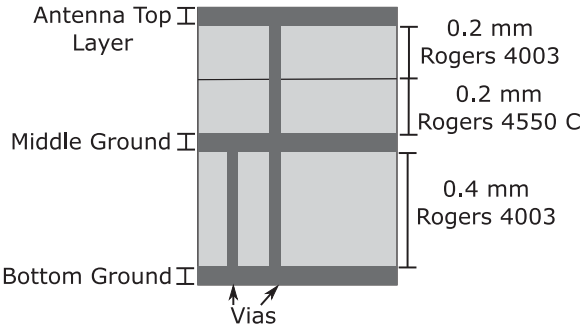

Fig. 7. UHF matching network for external and implant antennas.

penetrating the top layer. The implanted antenna is laminated with 1-mm-thick Teflon on the top and bottom of the stack, yielding a total size of 25 mm diameter and 3 mm thickness.

An HF spiral coil antenna forms the outer annulus on the implant antenna. It consists of three turns with inner radius 9.6 mm, outer radius 12.1 mm, trace width 0.4 mm, and interturn spacing 0.3 mm. As with the external coil antenna, these parameters were chosen via optimization using CST's frequency-domain solver to maximize the efficiency given the lossy dielectrics of the layered biomodel.

The implanted UHF antenna consists of an annular ring structure. The diameter of the ring is 14.6 mm, with an inner circular slot of 1.78 mm diameter. The ring is cut along a radius with a gap of 0.2 mm forming the feed point. The cut in the annular ring prevents the ring from forming a shorted turn that would otherwise be tightly coupled to the HF antenna surrounding it. This approach minimizes the unwanted loading and interaction between the HF and UHF antennas. As with the external antenna, lumped element matching networks shown in Figs. 5 and 6 are employed to reduce the required board area compared to printed (e.g., microstrip) matching elements.

IV. SAR Calculation

The time-domain solver module in CST was used to calculate the SAR at the implant site when the external antenna was driven with the maximum expected UHF transmitter power of 20 dBm at a frequency of 915 MHz. This value is derived from the link budget of our communication system. From an SAR point of view, the regulatory limits are driven by the UHF case, as tissue absorption at HF frequencies is much lower. As shown in Fig. 8, the peak UHF SAR value was 0.457 W/kg in 1 g of average mass, which is well below the regulatory limit of 1.6 W/kg.

V. Measurement Setup and Results

As shown in Fig. 9, testing of the antennas was performed in a cylindrical tank of diameter 30.4 cm filled with 3 L of 0.91% w/v saline solution serving as a tissue proxy. The antenna and connectors were protected from water infiltration by a thin ($\approx 70\ \mu$m) latex membrane and submerged to a depth of 11 mm below the surface of the liquid. The external antenna was separated by a varying air gap of 0–15 mm from the surface of the liquid, with 5 mm being the nominal air gap. Fig. 10 shows the measured performance of the HF antenna system as a function

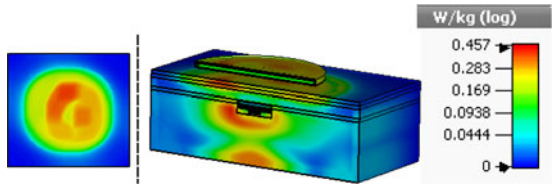

Fig. 8. Simulated UHF link SAR: (left) skin-surface top view; (right) cross section.

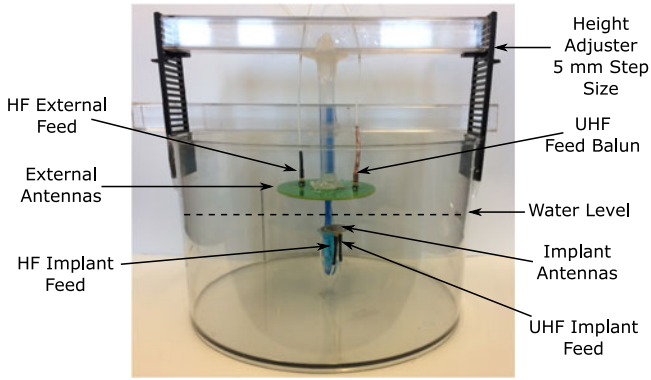

Fig. 9. Measured HF power transfer efficiency versus air gap.

TABLE I
Measured Versus Simulated Performance at 5-mm Nominal Air Gap

	Meas. (Saline)	Sim. (Saline)	Sim. (Layers)
UHF Link, 5 mm air gap			
Implant −10 dB BW (MHz)	898–916	908–916	906–917
External −10 dB BW (MHz)	870–955	891–936	889–932
Ins. Loss (dB), 910 MHz	37.65	38	25.7
HF Link, 5 mm air gap			
Implant −10 dB BW (MHz)	13.3–13.9	13.46–14.02	13.43–13.88
External −10 dB BW (MHz)	13.52–13.62	13.52–13.7	13.47–13.98
Ins. Loss (dB), 13.56 MHz	8	6	6.8

of the air gap, while Fig. 11 shows the measured performance of the UHF antenna system as a function of the air gap.

The measured and simulated results in the saline tissue proxy are compared in Table I, along with the simulated results in the layered biomodel. The biomodel indicates that expected performance in the layered tissue will be somewhat better than in the saline tissue proxy due to lower resistive losses in the protein and fat content of the tissue compared to pure saline.

The efficiency of the HF wireless power link was calculated using the transducer gain G_T [11], which is the ratio of power delivered to the load P_L to the power available from the source P_S, assuming conjugate matching at both ports

$$G_T = \frac{P_L}{P_S} = |S_{21}|^2 \frac{(1-|\tau_S|^2)(1-|\tau_L|^2)}{|1-\tau_S\tau_{\text{in}}|^2|1-S_{22}\tau_L|^2} \quad (1)$$

where $\tau_L = (Z_L - Z_0)/(Z_L + Z_0)$ is the reflection coefficient as seen looking toward the load, $\tau_S = (Z_S - Z_0)/(Z_S + Z_0)$ is the reflection coefficient as seen looking toward the source, and τ_{in} is the reflection coefficient as seen looking toward the

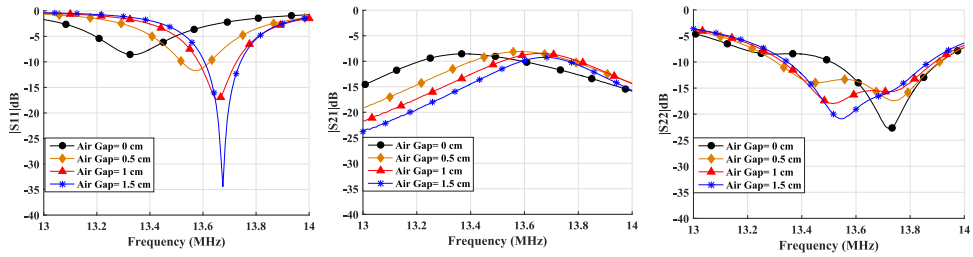

Fig. 10. Measured performance of HF antenna system. (a) External antenna $|S_{11}|$. (b) External to implant coupling $|S_{21}|$. (c) Implant antenna $|S_{22}|$.

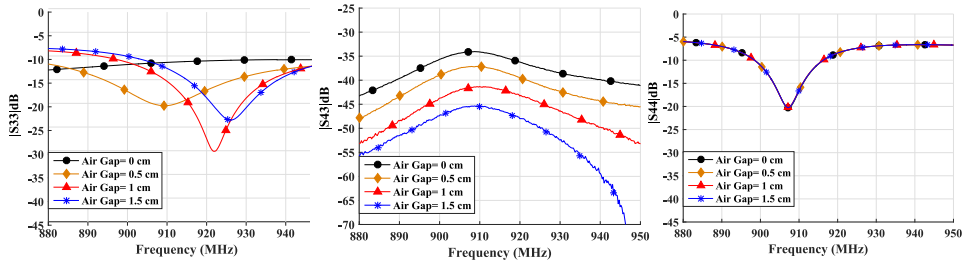

Fig. 11. Measured performance of UHF antenna system. (a) External antenna $|S_{33}|$. (b) External to implant coupling $|S_{43}|$. (c) Implant antenna $|S_{44}|$.

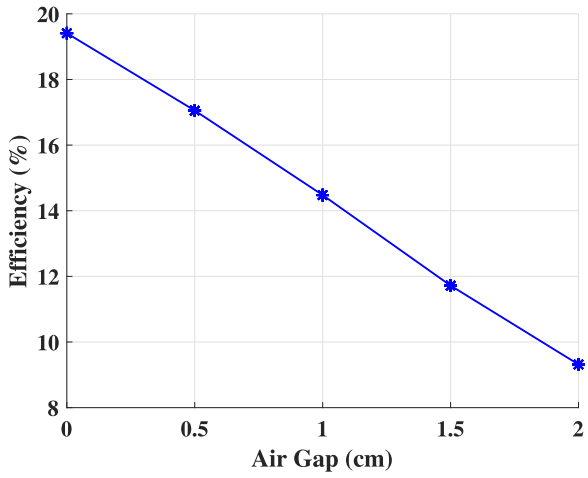

Fig. 12. Cylindrical tank saline solution experiment.

input of the two-port network. Fig. 12 shows the measured HF power transfer efficiency as a function of air gap; an efficiency of 17% is achieved at the nominal air gap of 5 mm. For the external antenna, the measured worst-case band-to-band coupling is −17 dB in the 902–928-MHz band and −49 dB at 13.56 MHz. For the implant antenna, the measured worst-case band-to-band coupling is −43 dB in the 902–928-MHz band and −55.6 dB at 13.56 MHz.

VI. Conclusion

This letter presents a dual-band HF and UHF (13.56 and 902–928 MHz) antenna system for implanted neural recording and/or stimulation devices. The antenna system is intended for dual-band systems where power is supplied to the implant via inductive coupling in the HF band, while data are transferred via UHF near-field coupling. We present both time- and frequency-domain simulation results for antenna performance and SAR in a layered tissue model, as well as experimental confirmation of antenna performance in a saline tissue proxy. With an implant depth of 11 mm and an air gap of 5 mm, the HF power link has a 17% measured power transfer efficiency in the HF band, inclusive of matching component loss, and a measured 38-dB insertion loss in the communication link over the 902–928-MHz band. Future work includes integrating the electronics with the implant-side antenna and carrying out further tests in an animal model. We also intend to modify this design to consider a flexible substrate.

References

[1] E. Moradi *et al.*, "Backscattering neural tags for wireless brain-machine interface systems," *IEEE Trans. Antennas. Propag.*, vol. 63, no. 2, pp. 719–726, Feb. 2015.

[2] S. O' Driscoll *et al.*, "A mm-sized implantable power receiver with adaptive link compensation," in *Proc. IEEE Int. Solid-State Circuits Conf. Dig. Tech. Papers*, Feb. 2009, pp. 294–295.

[3] T. Bjorninen *et al.*, "Design of wireless links to implanted brain-machine interface microelectronic systems," *IEEE Antennas. Wireless Propag. Lett.*, vol. 11, pp. 1663–1666, 2012.

[4] M. S. Chae *et al.*, "A 128-channel 6 mW wireless neural recording IC with spike feature extraction and UWB transmitter," *IEEE Trans. Neural Syst. Rehabil. Eng.*, vol. 17, no. 4, pp. 312–321, Aug. 2009.

[5] M. Zargham and P. G. Gulak, "Maximum achievable efficiency in near-field coupled power-transfer systems," *IEEE Trans. Biomed. Circuits. Syst.*, vol. 6, no. 3, pp. 228–245, Jun. 2012.

[6] A. S. Y. Poon *et al.*, "Optimal frequency for wireless power transmission into dispersive tissue," *IEEE Trans. Antennas Propag.*, vol. 58, no. 5, pp. 1739–1750, May 2010.

[7] H. Sun *et al.*, "Sequential activation of premotor, primary somatosensory and primary motor areas in humans during cued finger movements," *Clin. Neurophysiol.*, vol. 126, no. 11, pp. 2150–2161, Nov. 2015.

[8] R. Muller *et al.*, "A minimally invasive 64-channel wireless ECoG implant," *IEEE J. Solid-State Circuits*, vol. 50, no. 1, pp. 344-359, Jan. 2015.

[9] S. Gabriel *et al.*, "The dielectric properties of biological tissues: III. Parametric models for the dielectric spectrum of tissues," *Phys. Med. Biol.*, vol. 41, no. 11, pp. 2271–2293, Nov. 1996.

[10] M. Mark *et al.*, "SAR reduction and link optimization for mm-size remotely powered wireless implants using segmented loop antennas," in *Proc. IEEE Top. Conf. Biomed. Wireless Technol., Netw., Sens. Syst.*, Jan. 2011, pp. 7–10.

[11] D. M. Pozar, *Microwave Engineering*. New York, NY, USA: Wiley, 2005.